



HAL
open science

Global analysis of tungsten migration in WEST discharges using numerical modelling

Stefano Di Genova, Alberto Gallo, Luca Cappelli, Nicolas Fedorczak, Hugo Bufferand, Patrick Tamain, Juri Romazanov, Jorge Morales, Yannick Marandet, Christophe Guillemaut, et al.

► **To cite this version:**

Stefano Di Genova, Alberto Gallo, Luca Cappelli, Nicolas Fedorczak, Hugo Bufferand, et al.. Global analysis of tungsten migration in WEST discharges using numerical modelling. Nuclear Fusion, 2024, 10.1088/1741-4326/ad82f9 . hal-04739577

HAL Id: hal-04739577

<https://hal.science/hal-04739577v1>

Submitted on 16 Oct 2024

HAL is a multi-disciplinary open access archive for the deposit and dissemination of scientific research documents, whether they are published or not. The documents may come from teaching and research institutions in France or abroad, or from public or private research centers.

L'archive ouverte pluridisciplinaire **HAL**, est destinée au dépôt et à la diffusion de documents scientifiques de niveau recherche, publiés ou non, émanant des établissements d'enseignement et de recherche français ou étrangers, des laboratoires publics ou privés.



Distributed under a Creative Commons Attribution 4.0 International License

PAPER • OPEN ACCESS

Global analysis of tungsten migration in WEST discharges using numerical modelling










To cite this article: S. Di Genova *et al* 2024 *Nucl. Fusion* **64** 126049

View the [article online](#) for updates and enhancements.

You may also like

- [Evolution of pre-damaged ITER grade plasma facing components under WEST plasma exposure: smoothing and tungsten sources](#)
M. Richou, Y. Corre, M. Diez et al.
- [Separatrix parameters and core performances across the WEST L-mode database](#)
C. Bourdelle, J. Morales, J.F. Artaud et al.
- [MASTER OPTICAL POLARIZATION VARIABILITY DETECTION IN THE MICROQUASAR V404 CYG/GS 2023+33](#)
Vladimir M. Lipunov, E. Gorbovskoy, V. Kornilov et al.

Global analysis of tungsten migration in WEST discharges using numerical modelling

S. Di Genova¹ , A. Gallo² , L. Cappelli^{1,2} , N. Fedorczak², H. Bufferand², P. Tamain², J. Romazanov³ , J. Morales² , Y. Marandet⁴ , C. Guillemaut², J.P. Gunn², F. Clairet², S. Brezinsek³ , G. Ciraolo^{2,*} , E. Serre¹  and the WEST Team^a

¹ Aix-Marseille University, CNRS, Centrale Marseille, M2P2, 13013 Marseille, France

² CEA, IRFM, Saint-Paul-lez-Durance, F-13108, France

³ IEK-4, Forschungszentrum Jülich, 52425 Jülich, Germany

⁴ Aix-Marseille University, CNRS, PIIM, 13013 Marseille, France

E-mail: guido.ciraolo@cea.fr

Received 26 July 2024, revised 16 September 2024

Accepted for publication 3 October 2024

Published 15 October 2024



CrossMark

Abstract

Plasma discharges in the tungsten (W) Environment Steady-state Tokamak (WEST) are strongly impacted by W contamination. In WEST experiments, due to W contamination, the power radiated in the plasma (P_{Rad}) is on average, around 50% of the total power injected into the plasma (P_{TOT}). Furthermore, this radiated power fraction (f_{Rad}) is almost insensitive to plasma conditions. The causes behind this experimental trend are not fully understood. In this contribution, a 3D numerical model is used to analyze the W migration in the WEST boundary plasma in different plasma scenarios. The WEST experimental database is sampled to obtain a scan of simulation input parameters. These parameters mimic the WEST plasma conditions over a chosen experimental campaign. The simulation results are compared to WEST diagnostics measurements (reflectometry, Langmuir probes, and visible spectroscopy) to verify that the simulated plasma conditions are representative of the WEST database. The W contamination trend is analyzed: the W density (n_{W}) strongly decreases when the radial distance between the separatrix and WEST antennas (Radial Outer Gap, ROG) increases. On the other hand, at a given ROG, n_{W} increases proportionally with the power entering the scrape-off layer (P_{SOL}). P_{Rad} is estimated with a simple 0D model. For a fixed ROG, f_{Rad} is not sensitive to plasma conditions. These trends are qualitatively and, at times, quantitatively comparable to what is observed in WEST experiments: the simulated trends are related to the poorly screened W influx caused by the erosion of the main chamber Plasma-Facing Components. Thus, this numerical analysis suggests a possible interpretation of WEST experimental trends.

^a <http://irfm.cea.fr/en/west/WESTteam/>.

* Author to whom any correspondence should be addressed.



Original Content from this work may be used under the terms of the [Creative Commons Attribution 4.0 licence](https://creativecommons.org/licenses/by/4.0/). Any further distribution of this work must maintain attribution to the author(s) and the title of the work, journal citation and DOI.

Keywords: tokamak plasma, numerical modelling, impurity transport, WEST

(Some figures may appear in colour only in the online journal)

1. Introduction

The WEST tokamak is dedicated primarily to investigate long pulse operation in a full tungsten environment to prepare next step devices like ITER and DEMO. WEST is equipped with W-coated and bulk-W Plasma Facing Components (PFCs), and it is one of the machines used for testing the actively-cooled W divertor monoblocks designed for ITER.

During its first phase of operation (2017–2021) [1], WEST plasma discharges suffered from high levels of W contamination, which impacted the tokamak performances. The W contamination causes high power losses through radiation at the plasma core, affecting both the access to H-mode confinement as well as the amount of power entering the Scrape-Off Layer (SOL). Consequently, W contamination directly influences the heat flux reaching the divertor targets. The divertor monoblocks should be tested under a steady heat flux in the order of $\sim 10 - 20 \text{ MW m}^{-2}$. Nonetheless, W contamination has made this task very challenging. Therefore, studying W contamination represents a priority for WEST. Specifically, it is crucial to investigate the radiated power (P_{Rad}) trends found in the WEST database. Alongside the experimental effort to minimize W contamination, numerical modelling represents a complementary activity to study W migration mechanisms in WEST. Moreover, improving the numerical modelling of W migration in plasmas is an important preparatory activity for future tokamak machines. In the work described in this paper, numerical simulations are used for complementary investigations of the WEST experimental trends, in terms of W density (n_{W}) and P_{Rad} . The WEST database is analyzed to provide a set of characteristic simulation input parameters. These input conditions represent a partial coverage of the WEST operational domain, as discussed in the following. The codes SOLEDGE [2] and ERO2.0 [3] are used to perform 3D modelling of WEST boundary plasma and W migration under the considered conditions. Simulations are carried out with a realistic wall geometry. One of the key simulation input parameters is the radial distance (or Radial Outer Gap, ROG) between the separatrix and the main chamber limiters, i.e. the WEST antenna protections. The core P_{Rad} is estimated with a simple 0D model based on the WEST database and on simulation results. Simulations are compared to the WEST database to test whether the numerical model gives a realistic representation of WEST operational space. Finally, the n_{W} trends are analyzed, as well as the P_{Rad} ones. A detailed discussion on how simulation results can help interpret WEST experimental trends is included in the final part of the paper.

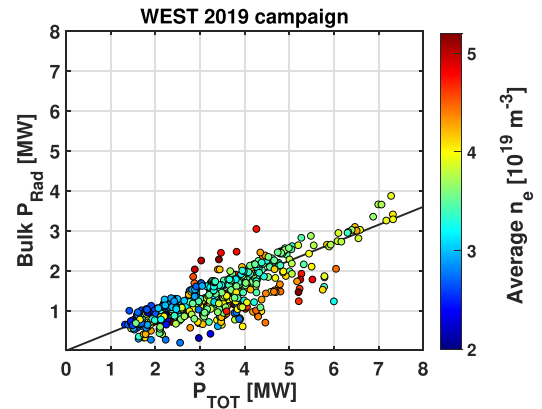


Figure 1. P_{Rad} in WEST plasmas as a function of P_{TOT} , in the diverted discharges of WEST 2019 campaign. The color refers to the core average n_e . f_{Rad} is given by the points slope. The grey line corresponds to $f_{\text{Rad}} = 45\%$.

2. W contamination in WEST

Throughout its first phase of operation, WEST performed plasma discharges characterized by a large radiated power fraction f_{Rad} . f_{Rad} is defined as:

$$f_{\text{Rad}} = \frac{P_{\text{Rad}}}{P_{\text{TOT}}} \quad (1)$$

where P_{TOT} is the total power injected in the discharge. Figure 1 shows P_{Rad} in WEST discharges, measured with bolometry [4]. P_{Rad} in the bulk plasma is shown as a function of P_{TOT} and the core average electron density (n_e , measured with interferometry [5, 6]). Each point in the figure represents a diverted discharge of the WEST campaign carried out in 2019 (also known as C4 [6]). In most of the pulses $f_{\text{Rad}} \approx 45\%$, with small sensitivity either to P_{TOT} or to n_e .

The causes of this particular trend are still unclear. The power entering the SOL (P_{SOL}) is the total one minus the power radiated in the bulk, here indicated with P_{Rad} . In other words, P_{Rad} is subtracted from the power effectively reaching the divertor targets. W contamination should be minimized to improve the tokamak performance. However, while the gross W erosion flux is measurable through visible spectroscopy, the net W flux is not measurable using WEST diagnostics. The net flux is defined as the gross W erosion flux minus the W flux screened by the plasma, which deposits to the wall before entering the separatrix. Furthermore, it is not trivial to disentangle the different phenomena that determine P_{Rad} in experiments. Finally, even though plasma conditions

govern W erosion and screening, f_{Rad} remains almost constant through WEST database. Thus, drawing conclusions exclusively based on experiments is very challenging. Consequently, numerical models are needed to gain insight into W contamination mechanisms in WEST.

3. The numerical model

Deploying numerical simulations of W migration presents several advantages. In simulations, quantifying the impact of the plasma scenarios on the plasma W content is straightforward. It is also possible to access both the W gross erosion and the net one. Finally, simulation inputs are independent from one another. Thus, it is possible to disentangle the effects of the parameters governing the problem. Trivially, the downside of these tools is the difficulty of assessing whether the results are realistic or not. For this reason, when drawing conclusions based on numerical analyzes, it is necessary to back up results with experimental data.

3.1. Modelling WEST 3D wall

In the 2019 campaign, all the WEST PFCs were either W-coated or bulk-W components (see figure 2(a)). The lower divertor, the upper divertor, and the baffle are axisymmetric PFCs. The other PFCs are toroidally localized objects. Among these, the closest ones to the plasma are the antennas and the limiter. The antennas are equipped with W-coated protections on the sides. The antenna protections act as limiters and protect the antennas from Plasma-Wall Interaction (PWI). The central part of the antennas does not face directly the plasma and is not W-coated. Figure 2(a) represents the WEST wall design.

It is shown that WEST is equipped with five antennas. Two are Lower Hybrid Current Drive (LHCD) antennas. The other three are Ion Cyclotron Resonance Heating (ICRH) antennas [7]. Moreover, an outboard limiter is also present in WEST. The toroidal distribution of these six PFCs is irregular. Furthermore, the distance between the plasma and any of these PFCs can change in between discharges. For example, in some WEST discharges, just the two LHCD antennas are deployed, with the other three antennas not facing the plasma.

It is rather complicated to deal with complex geometries in a numerical model. In this contribution it is adopted the wall model represented in figure 2(b). The axisymmetric PFCs of the model are faithful representations of the WEST ones. On the other hand, the toroidally localized PFCs are represented in a simplified way. In the model, the wall is equipped with four antennas, with a quarter of torus symmetry. The antenna protections (W-coated) are distinguished from the central part of the antennas (not W-coated). However, in the numerical model, the geometry of the antenna protections is simpler than the actual one. Moreover, the four antennas share the same radial position. These simplifications make the model less realistic. Nonetheless, the symmetry over a quarter of torus is preferred for this work, as it speeds simulations up. Moreover, the simplified antenna geometry is constrained by technical numerical limitations [8].

3.2. Background plasma modelling with SOLEDGE

The numerical model adopted in this work deploys the codes SOLEDGE and ERO2.0. A close description of the model can be found in [8–10]. SOLEDGE performs 3D simulations of the boundary plasma conditions with a multi-fluid model. In particular, in this work SOLEDGE is used to determine the spatial distribution of the electron density n_e , the deuterium (D) density n_D , the electron temperature T_e , the D temperature T_D and the plasma parallel velocity v_{\parallel} (under the ambipolar hypothesis [11]). The presence of light impurities is neglected in these SOLEDGE simulations, in order to reduce the computational time. The cross-field turbulent transport is accounted for on ‘large’ scales with diffusive processes. These cross-field diffusive phenomena are governed by the cross-field diffusion coefficient D_{\perp} , viscosity ν_{\perp} , electron conductivity χ_{\perp}^e , and ion conductivity χ_{\perp}^i . These parameters are considered to be spatially homogeneous and they are simulation inputs. In the simulations described in this contribution, SOLEDGE also computes the neutral D atoms distribution with a simple diffusive fluid model.

3.3. W migration modelling with ERO2.0

ERO2.0 simulates W erosion and transport with Monte Carlo methods. SOLEDGE simulations are used as background plasmas for the ERO2.0 runs. The background plasma provides the data ERO2.0 needs to compute the W erosion at the wall surface and to track the W particles trajectory in space. Also in ERO2.0 the cross-field turbulent transport is represented by a proxy diffusive process having diffusion coefficient D_{\perp} . In L-mode plasma conditions, the W erosion is majorly caused by the light impurities present in the plasma. Hence, in ERO2.0 simulations it is necessary to account for the presence of light species. Here, Oxygen (O) is used as a proxy for all the light impurities commonly present in tokamak plasmas (nitrogen, carbon, boron, etc). In the ERO2.0 version used in this work, light impurities are assumed to have a spatially homogeneous concentration. In WEST the light impurities concentration is experimentally estimated to be in the order of 1% [12]. In the ERO2.0 simulations carried out for this work, we assume that the Oxygen concentration is 3%. The W gross erosion flux scales linearly with this parameter, as the W erosion by D ions is negligible. The assumptions used for the O ionization states in simulations are further discussed in [8].

Both the SOLEDGE and the ERO2.0 computational domains include the SOL and a portion of the confined plasma. Inside the confined plasma, the computational domain does not cover the volume inside a certain magnetic flux surface. Here, this surface is referred to as the core-edge interface (i.e. the simulations inner boundary). Inside this boundary, the physical models used by the code are not very accurate, as a consequence of the low plasma collisionality in this region. Figure 3 shows an example of T_e distribution, computed by SOLEDGE. Figure 4(a) shows an example of W density (n_W) distribution, computed by ERO2.0. The figures also show the simulations inner boundary.

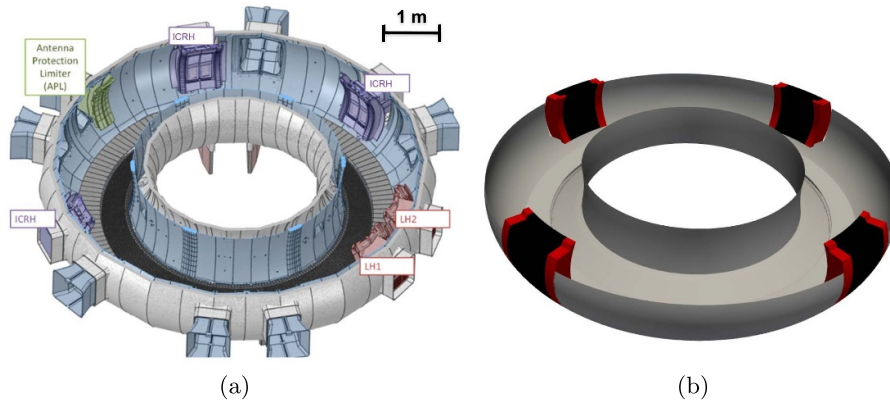


Figure 2. (a) WEST CAD design with scale. The wall is equipped with five antennas and one limiter. These PFCs are irregularly distributed along the toroidal direction. (b) Simplified WEST wall model for simulations. Four antennas are regularly distributed with a quarter of torus symmetry. The grey PFCs are the axisymmetric components. The red PFCs are the W-coated antenna protections. The black part of the antennas is not W-coated.

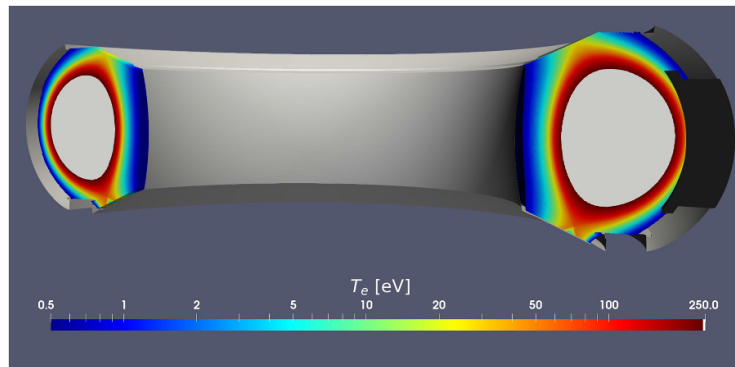


Figure 3. Electron plasma temperature T_e (on a portion of torus), obtained with a 3D SOLEDGE simulation in WEST geometry.

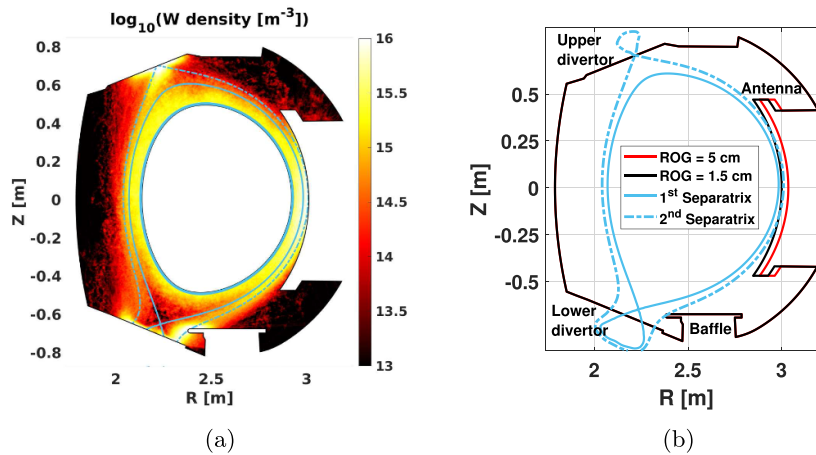


Figure 4. (a) Poloidal distribution (toroidal averaged) of tungsten density n_W , taken from a 3D ERO2.0 simulation in WEST geometry. (b) Intersection between the two separatrices and WEST PFCs, using the magnetic reconstruction adopted in simulations.

3.4. 0D model of the core radiated power

For an ion species i , the radiated power density can be calculated as $n_e n_i L_i(T_e)$. L_i is the ion cooling factor. W has a high L , with a peak around 2 keV: $L_W(2 \text{ keV}) \approx 5 \times 10^{-31} \text{ Wm}^3$. Since the computational domain in simulations does not cover the volume inside the inner boundary, here P_{Rad} in the core is approximated with the following 0D model:

$$P_{\text{Rad}}^{\text{Core}} = \int_V n_e n_W L_W(T_e) dV \approx \bar{n}_e \bar{n}_W L_W(2 \text{ keV}) V_{\text{plasma}} \quad (2)$$

where V_{plasma} is the core plasma volume. \bar{n}_W and \bar{n}_e are the average n_W and n_e values, respectively, in the core region. Equation (2) is a simplified model, but it can be useful in practical problems. For example, it is used to estimate n_W from bolometry measurements in experiments [13, 14]. WEST database gives a correlation between \bar{n}_e and the separatrix electron density n_e^{sep} [6]:

$$\bar{n}_e = 3.5 \times \left(\frac{n_e^{\text{sep}}}{10^{19}} \right)^{0.3} [10^{19} \text{ m}^{-3}] \quad (3)$$

that gives a further simplification to the 0D model. As in WEST $V_{\text{plasma}} \approx 15 \text{ m}^3$, P_{Rad} in the tokamak can be estimated as:

$$P_{\text{Rad}} = C \bar{n}_W \left(\frac{n_e^{\text{sep}}}{10^{19}} \right)^{0.3} \quad (4)$$

where the constant $C \approx 2.7 \times 10^{-16}$, \bar{n}_W is expressed in m^{-3} , and P_{Rad} is expressed in MW. In simulations, \bar{n}_W is taken equal to the average n_W on the inner boundary. This is equivalent to assuming a flat n_W distribution in the core (i.e. neglecting W accumulation). As discussed in the next section, n_e^{sep} is a simulation input. Thus, equation (4) can be readily used after the SOLEDGE and ERO2.0 runs. Although the model implies several simplifications, it is still very useful for estimating P_{Rad} in boundary plasma simulations.

4. Sampling the WEST database

The W contamination trends are analyzed simulating WEST plasmas in several scenarios. The final goal is gaining insight about the P_{Rad} trend found in the WEST database (discussed in section 2, see figure 1). Hence, a series of simulations that can represent the WEST database are carried out. This is done by performing a scan over different input parameters, which are chosen using the WEST database.

To represent the WEST operational domain, a scan over three main input parameters is performed. The parameters are P_{SOL} , the n_e value at the outer midplane (OMP) on the separatrix (n_e^{sep}), and the ROG. ROG is the radial distance between

the first separatrix and the closest antenna at the OMP (see for example figure 4(b)). The first two parameters are closely related to the main parameters controlling a WEST plasma discharge (P_{TOT} and the line integrated density), the latter is an important geometrical parameter that can be modified in between discharges. A reduced WEST database is used to analyze WEST data [14]. The WEST campaign performed in 2019 is taken as the reference campaign, as it is the WEST campaign composed of the largest number of discharges, and with the broadest operational domain extent so far [6]. In particular, the database is restricted to only the lower single-null D discharges from the WEST 2019 campaign in which more than 1 MW of external power is injected. Figure 5(a) shows the frequency of the values assumed by ROG in WEST discharges. The average ROG value is 2.5 cm, the most frequent value is around 2 cm, and in more than 95% of the discharges $\text{ROG} < 5 \text{ cm}$. In simulations, the representative values $\text{ROG} = 1.5, 3, 5 \text{ cm}$ are used. The last value is considered an upper limit. Figure 5(b) shows the frequency of the P_{SOL} values in WEST discharges: the average is 1.5 MW and in 91% of the discharges $P_{\text{SOL}} < 3 \text{ MW}$. In simulations, the power radiated by light impurities in the SOL is not computed. Hence, it is assumed that roughly 30% of the power crossing the separatrix is radiated in the SOL (since this value is on average $27\% \pm 1\%$ in the WEST database). Consequently, the values chosen for simulations are $P_{\text{SOL}} = 1, 1.5, 2 \text{ MW}$.

The values used for n_e^{sep} are 1.5, 2.0, $2.5 \times 10^{19} \text{ m}^{-3}$, plus the extra value $n_e^{\text{sep}} = 1.0 \times 10^{19} \text{ m}^{-3}$, for which simulations are carried out just at $P_{\text{SOL}} = 1 \text{ MW}$. This last case represents low power and low density discharges. n_e^{sep} is fixed through a feedback control on the neutral D injection rate in SOLEDGE. The diffusion coefficients are kept constant over simulations, their values are $D^\perp = \nu^\perp = 1.0 \text{ m}^2 \text{ s}^{-1}$, and $\chi_i^\perp = \chi_e^\perp = 2 \text{ m}^2 \text{ s}^{-1}$.

Plasma density n_e^{sep} values and radial transport coefficients are chosen *a priori*. Then, they are confirmed through the comparison of the results with WEST reflectometry.

The total number of backgrounds for the study is 30 (3 ROG values \times 3 P_{SOL} values \times 3 n_e^{sep} values + 3 \times 1 \times 1 cases for the low power and low density conditions, see table 1). The neutral diffusion coefficient is always $D_n = 1000 \text{ m}^2 \text{ s}^{-1}$ [15, 16].

5. Results comparison with WEST database

To test whether the conclusions drawn in this numerical analysis might be relevant for WEST experiments, simulation results are compared with WEST diagnostic measurements from the database. The diagnostics chosen for the comparison are the fast sweep reflectometry, the Langmuir probes, and the visible spectroscopy.

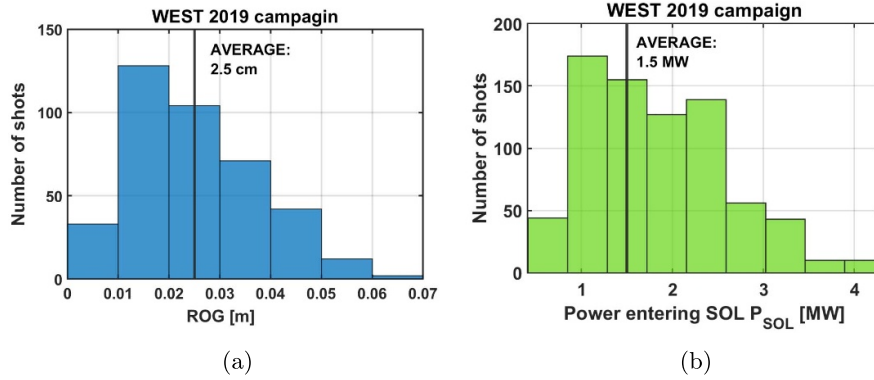


Figure 5. (a) ROG values frequency in WEST discharges. (b) P_{SOL} values frequency in WEST discharges.

Table 1. Summary of the simulation inputs. All the simulations are repeated with $\text{ROG} = 1.5, 3,$ and 5 cm, with a total of 30 different cases. In every simulation $D^\perp = \nu^\perp = 1 \text{ m}^2 \text{ s}^{-1}$, and $\chi_i^\perp = \chi_e^\perp = 2 \text{ m}^2 \text{ s}^{-1}$.

	$P_{\text{SOL}} = 1.0 \text{ MW}$	1.5 MW	2.0 MW
$n_e^{\text{sep}} = 1.0 \times 10^{19} \text{ m}^{-3}$	✓		
$1.5 \times 10^{19} \text{ m}^{-3}$	✓	✓	✓
$2.0 \times 10^{19} \text{ m}^{-3}$	✓	✓	✓
$2.5 \times 10^{19} \text{ m}^{-3}$	✓	✓	✓

5.1. Radial electron density profile: reflectometry

The n_e profiles at the OMP, computed by SOLEDGE, are compared to WEST reflectometry measurements [17]. Figure 6 shows the comparison: n_e is plotted as a function of the radial distance from the separatrix ($R - R_{\text{sep}}$).

The simulations data are taken at a toroidal angle equidistant from two consecutive antennas. The experimental separatrix radial position is taken as the arithmetical mean of the value estimated by the magnetic reconstruction performed by VACTH [18] and the one performed by NICE [19]. The orange line represents the average on WEST data at a given radial position. Moreover, at a given radial position, the yellow area represents the interval of the values bounded by WEST data standard deviation.

Simulations results are always included inside the experimental standard deviation, except for simulations with $n_e^{\text{sep}} = 2.5 \times 10^{19} \text{ m}^{-3}$. These last simulations can be seen as an upper limit for the density. The average n_e^{sep} value in WEST database is $\bar{n}_e^{\text{sep}} = 1.6 \times 10^{19} \text{ m}^{-3}$. Thus, the simulations with $n_e^{\text{sep}} = 1.5 \times 10^{19} \text{ m}^{-3}$ are the ones that resemble the average WEST measurements the most. Furthermore, it is possible to notice that P_{SOL} has no effect on the n_e profiles beyond the separatrix ($R - R_{\text{sep}} > 0$). On the other hand, ROG influences the profiles. In fact, the position of the antennas impacts the n_e drop, due to the particle sink at the wall. Beyond the antenna radial position (see the vertical line with the same line style of the considered simulation) n_e^{sep} drops quickly. At the considered toroidal position, the density SOL width λ_n^{SOL} in simulations is similar to the one of the curve given by WEST averaged measurements: $\lambda_n^{\text{SOL}} \approx 3$ cm. This value is in the order of magnitude of ROG. Thus, it is expected that the plasma interaction with antennas is not negligible.

5.2. Divertor plasma conditions: Langmuir Probes

The divertor plasma regime is particularly significant in evaluating the quality of the simulated background plasmas, as the WEST divertor is widely diagnosed by measurement systems.

Figure 7 shows the n_e profile at the lower divertor in SOLEDGE simulations. For fixed values of other inputs, increasing P_{SOL} slightly increases n_e , as a consequence of the higher recycling neutral flux. Increasing ROG also increases n_e , as a consequence of the reduced plasma flux reaching the antennas. In fact, the particle flux has to be redirected to the axisymmetric PFCs, increasing the recycling neutral flux as well. The cases at $\text{ROG} = 3$ cm and at $\text{ROG} = 5$ cm tend to be very similar to each other compared to the cases at $\text{ROG} = 1.5$ cm. This is mainly related to the radial position of the second separatrix, which is magnetically connected to the upper divertor. This is visible in figure 4(b): at the OMP the second separatrix distance from the primary separatrix is 2.6 cm. Hence, in the cases at $\text{ROG} = 3$ cm and $\text{ROG} = 5$ cm, the antennas are partially shadowed by the upper divertor and the baffle (that are connected to the second separatrix in the considered magnetic configuration). On the other hand, at $\text{ROG} = 1.5$ cm the antennas partially shadow the upper divertor and the baffle, as the second separatrix intercepts the antennas. Hence, the simulations at $\text{ROG} = 1.5$ cm are in a qualitatively different configuration compared to the simulations at $\text{ROG} = 3$ and 5 cm.

As expected, the divertor n_e increases with n_e^{sep} .

Figure 8 shows the T_e profiles at the lower divertor in the SOLEDGE simulations.

As expected, T_e increases with P_{SOL} , and decreases with n_e^{sep} . T_e slightly decreases with ROG, as a consequence of the slightly higher n_e .

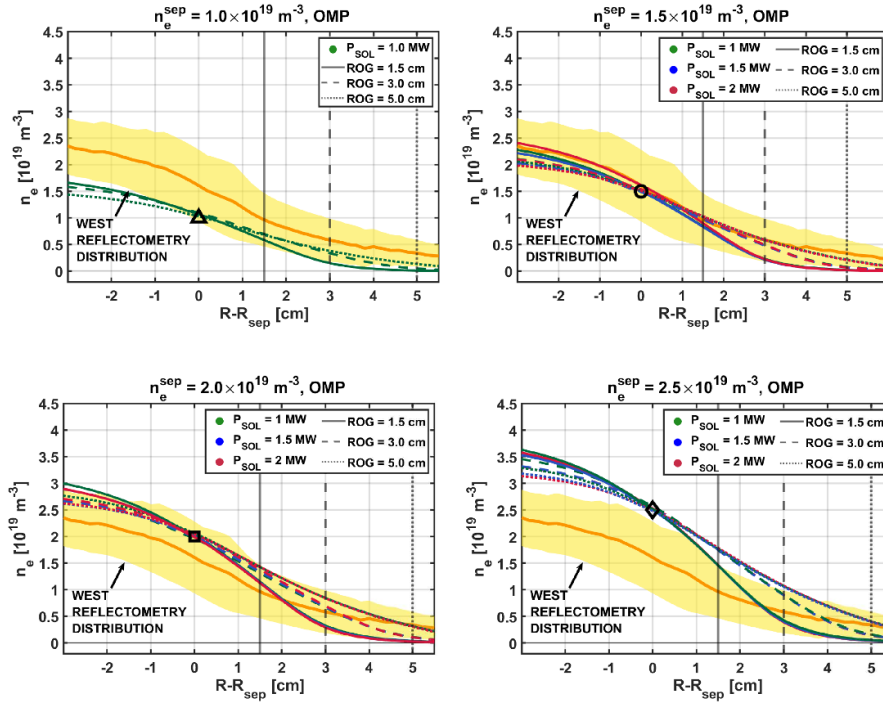


Figure 6. n_e profiles at the OMP, as a function of $R - R_{sep}$. n_e^{sep} values are readable in the titles and are represented by the markers. The orange line represents the average measurement on WEST reflectometry data for a given $R - R_{sep}$. Vertically, The yellow area covers the interval bounded by the WEST data standard deviation for a given radial position. The other lines represent SOLEDGE simulations. The vertical grey lines indicate the antennas radial position for simulations having the same line style.

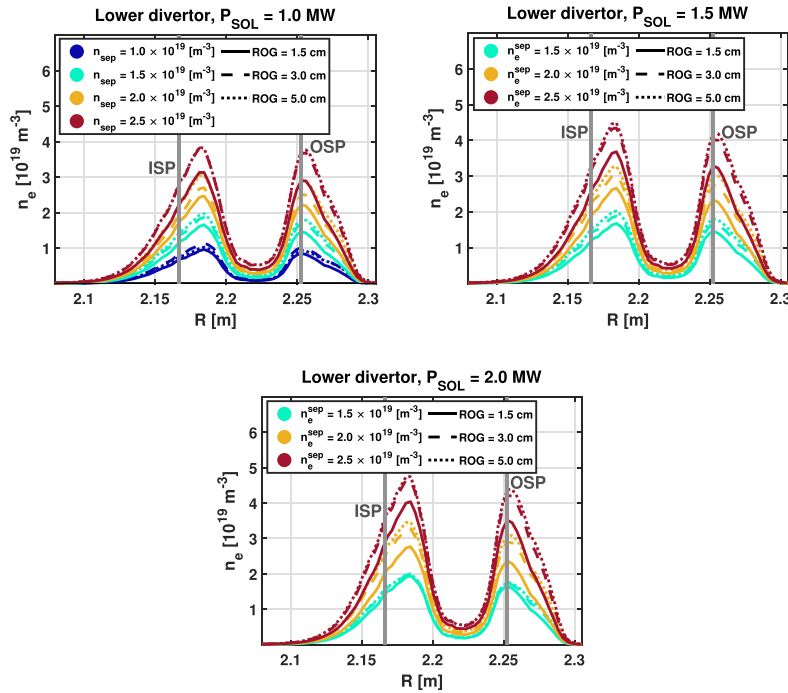


Figure 7. n_e profiles at the lower divertor targets in SOLEDGE simulations. Grey vertical lines denote the Inner and Outer Strike Points (ISP, and OSP) radial position.

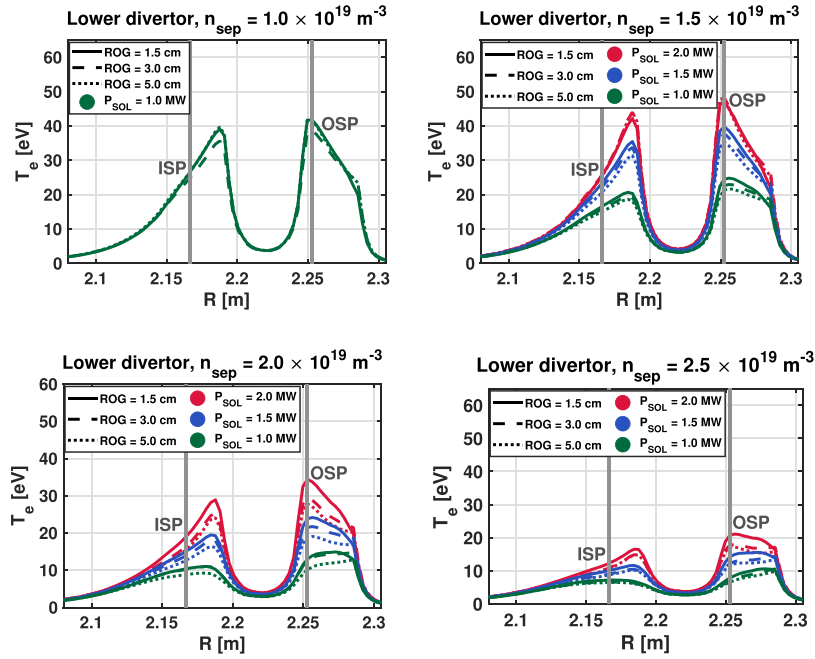


Figure 8. T_e profiles at the lower divertor targets in SOLEDGE simulations. Grey vertical lines denote the Inner and Outer Strike Points (ISP, and OSP) radial position.

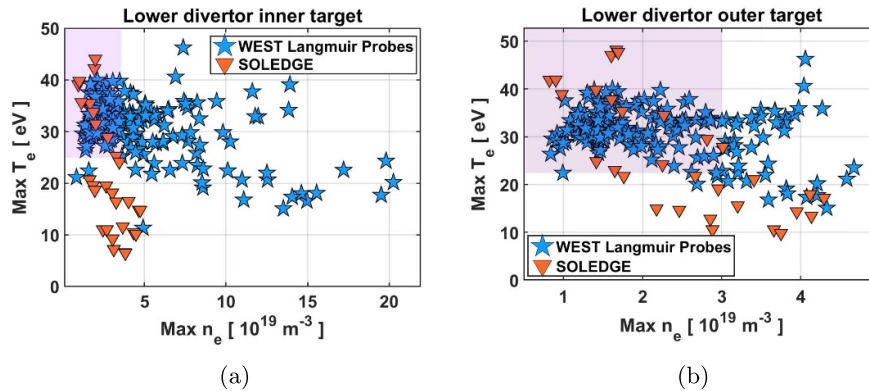


Figure 9. Maximum T_e as a function of the maximum n_e at the two lower divertor targets, in simulations and WEST experiments. The purple area represents the high T_e and low n_e regime.

After the analysis of the simulation trends, simulation results are compared with the WEST database. Figure 9 shows the comparison between SOLEDGE results and WEST Langmuir probes measurements [20] from the database. In particular, the peak T_e is plotted as a function of the peak n_e value for the two divertor targets.

At the inner target, the simulations match WEST conditions in the divertor regime characterized by $n_e < 3 \times 10^{19} \text{ m}^{-3}$ and $T_e > 25 \text{ eV}$ (most frequent regime, purple area in figure), but not in regimes characterized by higher n_e or lower T_e . On the other hand, at the outer target, SOLEDGE results match the WEST database regardless of the divertor regime. The inner-outer target divertor asymmetry, which can be seen in WEST database, may be related to plasma drifts [11], which are not included in these SOLEDGE simulations. Aside from rare

WEST discharges, with very high recycling at the inner target, the simulated n_e and T_e can be considered to be in acceptable agreement with the WEST database.

5.3. W gross erosion flux: visible spectroscopy

In order to guarantee that the simulated W erosion levels are similar to the ones seen in WEST, simulation results are compared with visible spectroscopy measurements [21]. In fact, this is the diagnostic used to indirectly measure the W erosion gross flux in WEST. The WI 400.9 nm line emission is related to neutral W atoms ionization [12]. The Photon Emission Coefficient (PEC) is taken from ADAS data [22], and used in ERO2.0 to compute the WI 400.9 nm volumetric photon emission. Applying synthetic diagnostics based on beam tracing

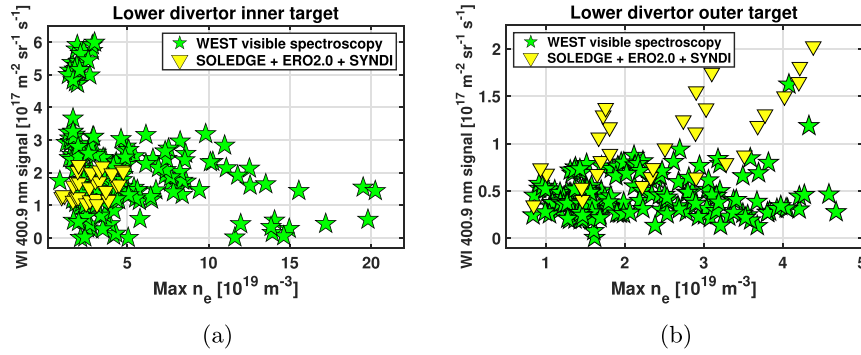


Figure 10. Maximum WI 400.9 nm visible spectroscopy signal VS maximum n_e at the two lower divertor targets, in simulations and WEST experiments.

(SYNDI [9, 23]), it is possible to compare simulation results with WEST visible spectroscopy data. In this way, we can compare simulations and experiments using the same physical quantity, that is the WI 400.9 photon flux, measured along the lines of sight of WEST visible spectroscopy cameras (simulated by SYNDI). This can be considered a proper way to compare WEST divertor gross erosion flux in experiments and simulations. On the other hand, the prompt deposition of W ions is self-consistently simulated by ERO2.0, but is not measured in WEST experiments. Therefore, it is not possible to perform a comparison between simulations and experiments of the net W erosion.

It should be pointed out that the estimated WI signal in simulations is proportional to the O concentration assumed in the model, as O is the main sputtering species in the ERO2.0 runs. Figure 10 shows the peak WI signal as a function of the peak n_e , for each of the lower divertor targets, in the WEST database and in simulations.

Once more, at the inner target, the model is not capable of obtaining all the different WEST regimes that emerged from experiments. On the other hand, at the outer target, simulations show the same trend as in the WEST database. Quantitatively, the difference between simulations and experiments lies within a factor that goes approximately from 1.5 in low density regimes, to 3 in high density cases. The larger difference in high density regimes can be decreased by tuning the O concentration in simulations. However, in that case, the low density cases would underestimate the W erosion. Nonetheless, the comparison is considered acceptable, as simulation results are in the same order of magnitude as experimental data. Moreover, it has to be noted that the introduction of synthetic diagnostics might further introduce errors in the model, regardless of the level of accuracy of the W erosion estimation.

6. Analysis of the W migration and the radiated power trends

As the comparison between simulations and experimental data is acceptable, an analysis of W migration trends can

be considered meaningful to WEST experiments. Figure 11 shows the average n_W value on the simulations inner boundary (i.e the core boundary). It is possible to notice the dependence on the different input parameters.

Increasing ROG, n_W strongly drops as a consequence of the weaker erosion of the antenna protections. The drop is particularly considerable, as in simulations the antenna protections are the PFCs responsible for most of the W contamination in the confined plasma. Increasing P_{SOL} results in a rise in n_W . The two quantities are almost proportional. This suggests that P_{Rad} may counter-stabilize P_{SOL} proportionally (through W contamination). This highlights the intricacy of trying to reduce the radiated fraction by increasing the injected power in experiments. Last, when increasing n_e^{sep} , n_W slightly reduces. This is mainly related to the increased W screening by plasma. However, P_{Rad} depends on the product $n_W n_e$. Hence, when increasing n_e^{sep} , P_{Rad} does not necessarily follow the same trend as n_W .

Once n_W trend is analyzed, and the effects of the simulation inputs are disentangled, P_{Rad} can be estimated with the 0D model (equation (4)). In figure 12, P_{Rad} is plotted as a function of the total power $P_{TOT} = P_{SOL} + P_{Rad}$.

It is shown that, for a fixed ROG, all simulations align on the same straight line ($P_{Rad} \propto P_{TOT}$). This indicates that f_{Rad} is fixed, with no sensitivity on P_{SOL} or n_e^{sep} . This particular behavior recalls what is observed in the WEST database (figure 1). Thus, in simulations f_{Rad} depends only on ROG.

As in simulations n_W is just proportional to the input O concentration, the proportionality $P_{Rad} \propto P_{TOT}$ would hold also in simulations assuming different O concentration values. In that case, f_{Rad} should be recalculated. It is not straightforward to forecast the sensitivity of the model to the O content if the O distribution is computed by SOLEDGE simulations.

As in simulations, the WEST database shows a dependence of f_{Rad} on ROG [7]. Figure 13 shows f_{Rad} as a function of ROG in both simulations and the WEST database.

WEST shows the same trend as in simulations but with weaker sensitivity to ROG. Particularly, the model estimates very low f_{Rad} for ROG = 5 cm compared to WEST experiments. It should be highlighted that the number of WEST discharges for ROG > 4 cm is less significant than the one for

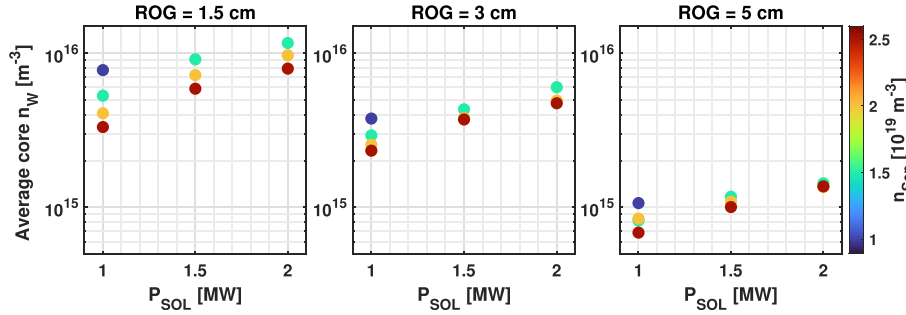


Figure 11. Average n_W values on the simulation core boundary, as a function of simulations input parameters.

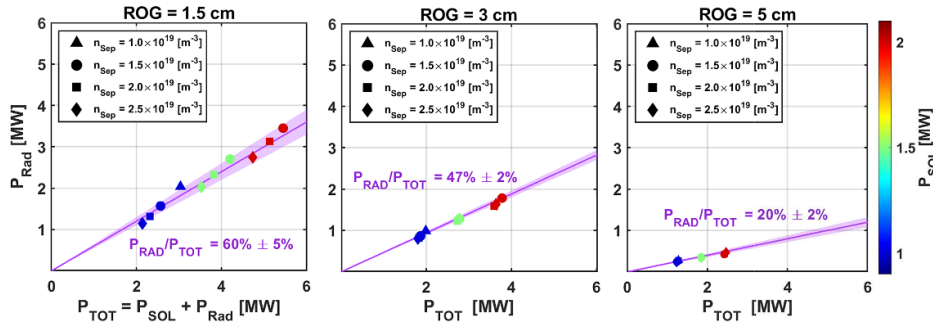


Figure 12. P_{Rad} as a function of P_{TOT} in simulations. At a given ROG, all simulations are enclosed in the purple area. This area is bounded by two constant f_{rad} values. The dark purple line corresponds to average f_{rad} in simulations, whose value is reported in the figure.

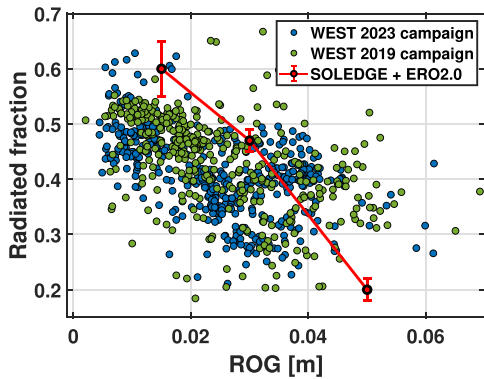


Figure 13. f_{Rad} as a function of ROG, in simulations, and in the WEST database.

ROG < 4 cm. The quantitative difference between the model and the experiments could be related to the different idealizations of the model. For instance, the simplified geometry of the antennas may affect the estimation of W prompt deposition. Furthermore, the error due to the simplified neutral model is expected to be larger where the neutral recycling is higher. Thus, the W screening at the divertor might be influenced by this idealization. It has to be pointed out that different numerical models suggest that WEST lower divertor W erosion is efficiently screened [9, 24, 25] and thus it might not largely influence the core W content. Further investigations are still ongoing to determine quantitatively these indications. Finally, the 0D core model used to estimate P_{Rad} is likely too raw, and can be improved by adopting more sophisticated integrated modelling in the future, as in [14].

Although the errors introduced by the model simplifications, the simulations show trends that match qualitatively, and at times quasi-quantitatively, the WEST experiments.

7. Conclusions

During its first phase of operation, the WEST experiment was characterized by intense levels of W contamination in its discharges. The radiated power caused by the W ions in the plasma core strongly impacted the tokamak power balance, influencing WEST performances. From the WEST database, it is possible to observe a trend characterized by high values of the radiated fraction $f_{\text{rad}} \approx 45\%$. This trend shows little sensitivity to the total injected power P_{TOT} , and to the average electron density \bar{n}_e .

In this work, a numerical model is used to investigate this particular WEST trend. SOLEDGE and ERO2.0 are used to perform 3D simulations of the boundary plasma conditions and the W migration, respectively. The wall model is a faithful representation of the WEST axisymmetric PFCs, and a simplified representation of the WEST antennas. A 0D model is adopted to estimate the core radiated power P_{Rad} from simulation results. A scan over different simulation input parameters is performed. These inputs are the power entering the SOL P_{SOL} , the midplane separatrix electron density n_e^{sep} , and the radial distance between the separatrix and the antennas (ROG). In order to analyze the WEST operational domain, the values used for these inputs are sampled from a WEST reduced database. In particular, the WEST 2019 campaign is taken as a reference. Simulation results are compared to different WEST

diagnostics, in order to test how much the numerical analysis is relevant for WEST conditions. Simulations are in very good agreement with WEST reflectometry data. The comparison with Langmuir probes measurement shows that the divertor conditions in simulations are similar to the WEST one. Nonetheless, the divertor target asymmetry, present in some WEST discharges, cannot be reproduced in these simulations. Similar conclusions can be obtained from the comparison of simulation results with the WI visible signal at the WEST divertor. As simulations are in acceptable agreement with the WEST database, W contamination trends are analyzed. Simulations show how the W density n_W inside the separatrix is almost proportional to P_{SOL} . Increasing n_e^{sep} reduces n_W , as a consequence of the stronger W screening by plasma. Nevertheless, P_{Rad} depends on the product $n_e n_W$. Hence, the decreasing of n_W is counterbalanced by the increased n_e^{sep} . ROG heavily impacts n_W , as the erosion of the antenna protections causes most of W plasma contamination in simulations. For a fixed ROG value, P_{Rad} is proportional to P_{TOT} . f_{Rad} just depends on ROG, with no sensitivity to P_{SOL} or n_e^{sep} . This particular trend is similar to what is observed in WEST. This trend in simulations is explained in the following way: simulations show that n_W is proportional to P_{SOL} . Moreover, the enhanced W screening, caused by higher n_e conditions, does not affect the product $n_e n_W$. For a fixed ROG, these two effects combine, resulting in no f_{Rad} sensitivity to P_{SOL} and n_e . This explanation could be a valid interpretation of the WEST experiments trend as well. Finally, both the WEST database and the numerical analysis show the same qualitative trend of the f_{Rad} dependence on ROG.

The results presented in this contribution suggest a possible interpretation of the f_{Rad} trends in WEST experiments. In fact, this work highlights the possibility that the erosion of the main chamber PFCs (Antenna protections) might dominate the W contamination in WEST. Moreover, simulations suggest that the W screening at these components could be low enough to be weakly influenced by the plasma conditions. In order to weaken the erosion of the antenna protections, it is necessary that $ROG \gg \lambda_n^{SOL}$. This might be achieved by either increasing ROG or improving the confinement of the plasma.

Acknowledgment

This work has been carried out within the framework of the EUROfusion Consortium, funded by the European Union via the Euratom Research and Training Programme (Grant Agreement No. 101052200 - EUROfusion). Views and opinions expressed are however those of the author(s) only and do not necessarily reflect those of the European Union or the European Commission. Neither the European Union nor the European Commission can be held responsible for them.

ORCID iDs

S. Di Genova  <https://orcid.org/0000-0003-4416-5600>
 A. Gallo  <https://orcid.org/0000-0002-7472-7830>
 L. Cappelli  <https://orcid.org/0000-0002-7198-7864>
 J. Romazanov  <https://orcid.org/0000-0001-9439-786X>
 J. Morales  <https://orcid.org/0000-0002-3140-0504>
 Y. Marandet  <https://orcid.org/0000-0002-9970-538X>
 S. Brezinsek  <https://orcid.org/0000-0002-7213-3326>
 E. Serre  <https://orcid.org/0000-0002-3174-7727>

References

- [1] Bucalossi J. *et al* 2022 Operating a full tungsten actively cooled tokamak: overview of WEST first phase of operation *Nucl. Fusion* **62** 042007
- [2] Bufferand H. *et al* 2019 Three-dimensional modelling of edge multi-component plasma taking into account realistic wall geometry *Nucl. Mater. Energy* **18** 82–86
- [3] Romazanov J. *et al* 2019 Beryllium global erosion and deposition at JET-ILW simulated with ERO2.0 *Nucl. Mater. Energy* **18** 331–8
- [4] Devynck P. *et al* 2021 Calculation of the radiated power in west *J. Phys. Commun.* **5** 095008
- [5] Gil C. *et al* 2019 Renewal of the interfero-polarimeter diagnostic for WEST *Fusion Eng. Des.* **140** 81–91
- [6] Bourdelle C. *et al* 2023 Separatrix parameters and core performances across the WEST I-mode database *Nucl. Fusion* **63** 056021
- [7] Urbanczyk G. *et al* 2021 RF wave coupling, plasma heating and characterization of induced plasma-material interactions in WEST I-mode discharges *Nucl. Fusion* **61** 086027
- [8] Di Genova S. *et al* 2023 First 3D modelling of tungsten erosion and migration in WEST discharges adopting a toroidally non-symmetric wall geometry *Nucl. Mater. Energy* **34** 101340
- [9] Di Genova S. *et al* 2021 Modelling of tungsten contamination and screening in WEST plasma discharges *Nucl. Fusion* **61** 106019
- [10] Gallo A. *et al* 2020 First efforts in numerical modeling of tungsten migration in WEST with SolEdge2D-EIRENE and ERO2.0 *Phys. Scr.* **T171** 014013
- [11] Stangeby P.C. 2000 *The Plasma Boundary of Magnetic Fusion Devices (Series in Plasma Physics and Fluid Dynamics)* (Taylor & Francis)
- [12] van Rooij G.J. *et al* 2020 Tungsten divertor sources in WEST related to impurity inventory and local plasma conditions *Phys. Scr.* **T171** 014060
- [13] Fedorczak N. *et al* 2014 Tungsten transport and sources control in JET ITER-like wall H-mode plasmas *J. Nucl. Mater.* **463** 12
- [14] Ostuni V. *et al* 2022 Core radiative collapse characterisation and integrated modelling in WEST plasmas *Nucl. Fusion* **62** 106034
- [15] Horsten N. *et al* 2017 Assessment of fluid neutral models for a detached iter case *Nucl. Mater. Energy* **12** 869–75
- [16] D'Abusco M. 2022 Numerical modelling of the core-boundary turbulent transport in tokamaks in realistic geometry

- through advanced numerical methods *PhD Thesis* Aix-Marseille Univ.
- [17] Clairet F. *et al* 2010 Fast sweeping reflectometry upgrade on Tore Supra *Rev. Sci. Instrum.* **81** 10D903
- [18] Faugas B., Blum J., Boulbe C., Moreau P. and Nardon E. 2014 2D interpolation and extrapolation of discrete magnetic measurements with toroidal harmonics for equilibrium reconstruction in a tokamak *Plasma Phys. Control. Fusion* **56** 114010
- [19] Faugas B. *et al* 2020 An overview of the numerical methods for tokamak plasma equilibrium computation implemented in the NICE code *Fusion Eng. Des.* **160** 112020
- [20] Gunn J.P. *et al* 2007 Evidence for a poloidally localized enhancement of radial transport in the scrape-off layer of the Tore Supra tokamak *J. Nucl. Mater.* **363–365** 484–90
- [21] Meyer O. *et al* 2018 Visible spectroscopy diagnostics for tungsten source assessment in the WEST tokamak: first measurements *Rev. Sci. Instrum.* **89** 10D105
- [22] Eksaeva A. *et al* 2017 ERO modelling of tungsten erosion in the linear plasma device PSI-2 *Nucl. Mater. Energy* **12** 03
- [23] Gallo A. *et al* 2020 Interpretative transport modeling of the WEST boundary plasma: main plasma and light impurities *Nucl. Fusion* **60** 126048
- [24] Maeker J.B. *et al* 2022 OEDGE modeling of far-SOL tungsten impurity sources and screening in WEST *Nucl. Mater. Energy* **33** 101309
- [25] Cappelli L. *et al* 2023 Study of the erosion and redeposition of W considering the kinetic energy distribution of incident ions through a semi-analytical model *Plasma Phys. Control. Fusion* **65** 095001